Received: 20 November 2018 | Revised: 1 April 2019 | Accepted: 14 May 2019

DOI: 10.1002/joc.6162

RESEARCH ARTICLE

International Journal of Climatology RMetS

Temporal and spatial variations of convection and precipitation over the Tibetan Plateau based on recent satellite observations. Part I: Cloud climatology derived from *CloudSat* and *CALIPSO*

Julia Kukulies[1] | **Deliang Chen**[1] | **Minghuai Wang**[2]

[1]Regional Climate Group, Department of Earth Sciences, University of Gothenburg, Gothenburg, Sweden

[2]School of Atmospheric Sciences, Nanjing University, Nanjing, China

Correspondence
Deliang Chen, Department of Earth Sciences, University of Gothenburg, Box 460, 405 30 Gothenburg, Sweden.
Email: deliang@gvc.gu.se

Funding information
Chinese Academy of Sciences, Grant/Award Number: XDA2006040103; National Natural Science Foundation of China, Grant/Award Numbers: 91537210, 91744208, 41621005, 41575073; Swedish Foundation for International Cooperation in Research and Higher Education, Grant/Award Number: CH2015-6226; Vetenskapsrådet, Grant/Award Numbers: 2014-5320, 2017-03780; Swedish Research Council, Grant/Award Numbers: 2017-03780, 2014-5320; Ministry of Science and Technology of China, Grant/Award Number: 2017YFA0604002; Swedish STINT, Grant/Award Number: CH2015–6226; Swedish National Space Agency, Grant/Award Number: SNSA: 188/18

Abstract

This sequence of papers, consisting of two parts, examines temporal and spatial variations of convection and precipitation over the Tibetan Plateau (TP) based on recent satellite observations. Here in Part 1, seasonal and diurnal variations of cloud vertical structure and cloud properties have been derived from four combined *CloudSat* and Cloud-Aerosol Lidar and Infrared Pathfinder Satellite Observation satellite data sets and compared between three subregions in the TP which are marked by different dominating large-scale atmospheric circulations and moisture sources. The results show that the plateau is generally dominated by low-level single-layer clouds and stratiform cloud types. Cloud occurrence frequencies peak during the summer monsoon season between May and September and are generally higher during daytime compared with nighttime in all the three subregions. The fraction of detected ice cloud layers in the TP domain exceeds 50% during all months and 80% between January and April. While ice cloud layers occur as altostratus clouds in the westerly dominated north and transition zone, high-level cirrus cloud occurs frequently accompanied by lower level cumulus clouds in the monsoon-dominated south, especially during nighttime. This study complements previous satellite observations of clouds over the TP and reveals firstly the high contribution of stratiform ice cloud layers in the westerly dominated north, secondly the importance of the monsoon season which outweighs day-night differences and affects the examined cloud parameters in all regions and finally the significant regional differences of cloud characteristics within the plateau. It is therefore suggested to focus on the relative importance of stratification, mesoscale convective systems and advection in future studies on hydro-climatic changes in the TP region.

KEYWORDS

climatology, cloud vertical structure, *CloudSat*, ice clouds, Indian summer monsoon, Tibetan Plateau, westerlies

Abbreviations: CCN, cloud condensation nuclei; CFAD, contoured-frequency-by-altitude diagram; CPR, cloud profiling radar; IN, ice condensation nuclei; TP, Tibetan Plateau.

1 | INTRODUCTION

The Tibetan Plateau (TP) is also referred to as the third Pole, because it stores the largest amounts of fresh water after the Arctic and Antarctica (Yao *et al.,* 2012, 2018). With an average elevation above 4,000 m a.s.l. over an area of 5 million km^2 (Yao *et al.,* 2012), it is the most extensive high altitude region of the world. It represents also one of the most sensitive regions to climate change, because intensive surface heating which is reinforced by different feedback mechanisms have led to enhanced atmospheric warming, glacier retreat and an accelerated hydrological cycle (Bibi *et al.,* 2018).

Pepin *et al*. (2015) describe the TP as an outstanding example for elevation-dependent warming (EDW) and Liu *et al*. (2009b) suggest that cloud–radiation interactions are one of the underlying mechanisms that contribute to this observed effect of accelerated warming at higher elevations over the TP. Station observations and model simulations suggest that decreasing cloud occurrences during daytime have reduced the cloud albedo of the region and this in combination with increasing low-level clouds during nighttime led to an increase of minimum temperatures (Duan and Wu, 2006). However, because the effect of clouds on the regional climate and its linkages to precipitation are dependent on different cloud macrophysical and microphysical properties (Boucher *et al.,* 2013), it is crucial to understand the temporal and spatial variations of these in addition to the total cloud amount (Berry and Mace, 2015). Spaceborne active remote sensing provides a useful tool for climatological studies of various cloud parameters at a high spatio-temporal resolution (including the vertical dimension) (Stephens *et al.,* 2002), especially in regions such as the TP where meteorological stations are sparsely distributed.

Several previous studies have used active remote sensing techniques to examine convection over the TP (Ruethrich *et al.,* 2013; Li and Zhang, 2016; Yan *et al.,* 2016; Pan *et al.,* 2017; Yan *et al.,* 2017; Hu *et al.,* 2017; Shang *et al.,* 2018). Li and Zhang (2016) have found that cumulus clouds from shallow convection are among the most common cloud types over the TP, especially between June and August, when the summer monsoon dominates the moisture transport to the region. Climate model simulations suggest that these cumulus clouds hamper the development of stratiform cloud layers over large areas (Li and Zhang, 2017). Whereas deep convection cells seem to dominate the southeastern parts of the plateau (Yaodong *et al.,* 2008; Luo *et al.,* 2011; Xu and Zipser, 2011) and contribute to the transport of moisture and precipitation over the southern mountain ranges (Dong *et al.,* 2016), convection is generally shallow compared with the surrounding regions (Luo *et al.,* 2011). Yan *et al*. (2017) describe a *compression effect*, referring to the low vertical extents of observed cloud layers over the TP. Since these result from both relatively low cloud base and top heights above ground level, clouds have a net cooling effect in the region (Yan *et al.,* 2017). However, while the above-named studies have mainly focused on the summer monsoon season, there is insufficient knowledge about the seasonality and diurnal variations of cloud types other than cumulus. The occurrence of ice clouds have, for example, only been addressed in a few studies based on first-generation passive satellites (Chen and Liu, 2005) or measurements from single stations (He *et al.,* 2013). Moreover, regional differences of cloud occurrences and properties within the TP as well as the linkages between convection and precipitation remain unexplored to a large extent. For these reasons, recent satellite observations from *CloudSat* and *CALIPSO* (Cloud-Aerosol Lidar and Infrared Pathfinder Satellite Observation) were used in this study to examine seasonal and diurnal variations of cloud characteristics in three subregions of the TP. The paper serves as a pilot study for future research on convection processes over the TP and provides a general overview of cloud variations in the region.

We will proceed in the following way. The used data products and processing of the four combined *CloudSat-CALIPSO* profile data are described in Sections 2 and 3. The satellite-derived cloud climatology consists of cloud frequencies, cloud types, cloud vertical structure and ice cloud occurrences and is presented in Section 4. Section 5 summarizes and discusses the three key findings of this study.

2 | DATA SETS

CloudSat (Stephens *et al.,* 2002) and *CALIPSO* (Winker *et al.,* 2009) belong to the A-train constellation, which is a satellite mission consisting of five Earth observing sun-synchronous satellites with the same polar orbit. The satellites fly at an altitude of 705 km above Earth's surface and orbit the globe between 13 and 16 times per day (14.56 orbits/day on average). However, only two of the daily orbits pass the TP each day at same local solar time, whereby one overpass occurs during daytime (ca. 13.30 local time) and the other during nighttime (ca. 1.30 local time). *CloudSat* and *CALIPSO* have thus a revisit time of about 14 days and some locations of the TP are not covered at all.

The Cloud Profiling Radar (CPR) is the measuring sensor of *CloudSat* and records the radar reflectivity of three-dimensional cloud systems. It operates at 94 GHz (where the absorption of atmospheric gases is small) with a time interval of 0.32 s and has the capacity to identify and penetrate optically thick clouds. Cloud-Aerosol Lidar with Orthogonal Polarization (CALIOP) is a spaceborne polarization lidar sensor on CALIPSO which operates at a frequency of 10 Hz

and is, in contrast to CPR, very sensitive to optically thin clouds. It is able to measure the depolarization ratio at 532 nm and the attenuated backscattering coefficient at both 532 nm and 1,064 nm. This capability is useful for the determination of cloud particle phase (Heymsfield *et al.,* 2005) and for the detection of hydrometeors with echos below the CPR detection minimum of −30 dBZ (Stephens *et al.,* 2002). Owing to the complementary skills of CALIOP and CPR, it was chosen to derive the cloud climatology in this study from combined CPR and CALIOP satellite retrievals.

The cloud profile data products 2B-GEOPROF (2006–2011), 2B-GEOPROF-LIDAR (2006–2011), 2B-CLDCLASS-LIDAR (2007–2010) and 2C-ICE (2007–2010) have been obtained from the NASA server (ftp.cloudsat.cira.colostate.edu) and processed as described in Section 3. The used data products and examined cloud parameters for the respective periods are summarized in Table 1. A more detailed description of the respective data sets and underlying retrieval algorithms is given by Mace (2008), (Sassen and Wang, 2008) and Mace and Deng (2011). The sampled hydrometeor profiles in 2B-GEOPROF, 2B-GEOPROF-LIDAR and 2C-ICE are aggregated in data granules of one orbit, where each profile consists of 125 vertical bins corresponding to 0.24 km. On the contrary, the parameter values of 2B-CLDCLASS-LIDAR are given for each detected vertical cloud layer in one profile. A cloud layer is defined as a vertically and horizontally connected cloud cluster and CPR can detect up to five cloud layers in one profile (Stephens *et al.,* 2002). All cloud profiles are recorded with a horizontal resolution of 1.1 km along track and 1.3 km across track (Stephens *et al.,* 2002).

3 | DATA PROCESSING OF CLOUD PROFILES

In order to identify possible day–night differences, the data granules have first been separated according to the two different overpass times (Section 2). The data have further been aggregated into monthly grids, following Li and Zhang (2016) who found that a 1° × 1° grid is the optimal resolution for an adequate amount and equal distribution of profile samples over the grid cells. Figure 1 illustrates the average number of monthly profile samples over the TP in each grid cell and Table 2 shows the total amount of profile samples for the period 2006–2011 in the different subdomains, separated into daytime and nighttime.

Cloud fractions have been calculated as suggested by Zhang *et al*. (2014). In order to include hydrometeors that are only detected by CPR or CALIOP, the cloud fraction is set to 100%, when the CPR cloud mask in 2B-GEOPROF is ≥30 (corresponding to a high-confidence cloud detection) and when radar reflectivity is above the CPR minimum detection level of −30 dBZ. Otherwise, the value is replaced by the lidar fraction of hydrometors in one radar volume, as provided in the 2B-GEOPROF-LIDAR product (Table 1). A profile is determined to be cloudy if it contains hydrometeor detections by either radar and/or lidar. Cloud layer occurrences refer, by contrast, only to vertically and horizontally connected cloud detections (c.f. Section 2). Relative occurrence frequencies of cloud layer properties (e.g., cloud layer amount in Section 4.a and ice cloud occurrences in Section 4.d) describe the average fractions of the respective parameter when a profile has been found to be cloudy.

In order to identify regional differences of cloud characteristics within the TP and to account for the different impact of large-scale atmospheric circulation and associated moisture transport, a framework for regionalization introduced by Yao *et al.* (2013) has been used in this study. Since the hydro-climate of the TP is mainly affected by two atmospheric large-scale circulation patterns, namely the mid-latitude westerlies and the Indian and East Asian summer monsoon (Yao *et al.,* 2013; Liu *et al.,* 2016), the plateau is divided into three distinct zones based on ice core reconstructions (Yao *et al.,* 2013). Whereas it is assumed that the domain north of latitude 35°N is primarily affected by the moisture transport through westerlies, the domain south of 30°N is, according to this framework, dominated by the monsoon circulation (Figure 2). The central TP between latitudes 30°N and 35°N is referred to as the transition zone and

TABLE 1 Overview of combined *CloudSat-CALIPSO* data products used in this study

Satellite	Data product	Parameters	Sensor	Resolution	Period
CloudSat	2B-GEOPROF	CPR mask, radar reflectivity	CPR	0.24 km vertical, 1.3 × 1.7 km horizontal	2006–2011
CloudSat, CALIPSO	2B-GEOPROF-LIDAR	Lidar cloud fraction, layer amount	CPR, CALIOP	0.24 km vertical, 1.3 × 1.7 km horizontal	2006–2011
CloudSat, CALIPSO	2B-CLDCLASS-LIDAR	Layer type, particle phase, layer base and top height	CPR, CALIOP	5 layers vertical, 1.3 × 1.7 km horizontal	2007–2010
CloudSat, CALIPSO	2C-ICE	Column-integrated optical depth	CPR, CALIOP	0.24 km vertical, 1.3 × 1.7 km horizontal	2007–2010

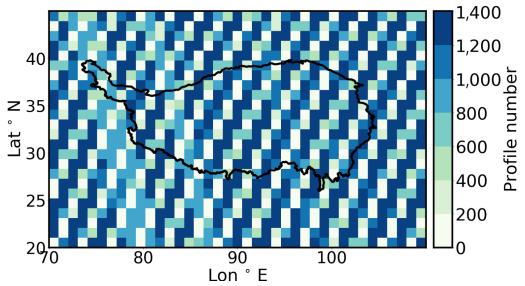

FIGURE 1 Average number of monthly grid samples in 1° × 1° based on 2B-GEOPROF/2B-GEOPROF-LIDAR (2006–2011). Grid cell values vary between a few and 1,400. According to Li and Zhang (2016), the optimal compromise between profile sample amount per grid and an equal distribution over the grid cells is achieved in the 1° × 1° resolution grid

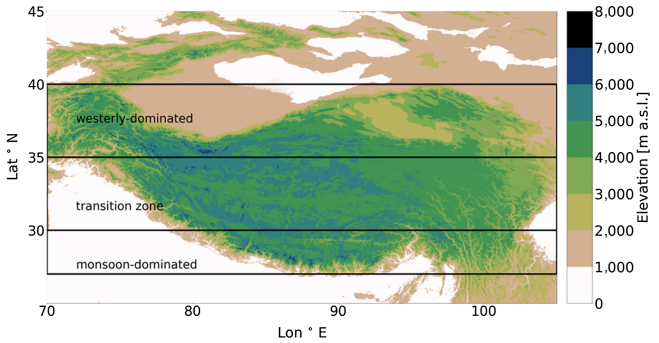

FIGURE 2 Topography of the TP and illustration of the three subregions based on impact of large-scale moisture transport according to Yao *et al*. (2013). Locations within the domain 27°–40°N, 70°–105°E and above 3,000 m a.s.l. are in this study defined as the TP

is affected by both large-scale circulation systems (Figure 2). It should also be noted, that only locations above 3,000 m a.s.l. are defined as the TP. The study has further focused on the two seasons, where the respective large-scale circulation system prevail: (a) May–September for the monsoon season (Wang, 2002) and (b) October–April for the westerly season, which refers to the dry season between monsoon dissipation and onset, where the strongest midlatitudes westerlies occur (Liu *et al.,* 2016).

4 | RESULTS

4.1 | Total cloud occurrences and cloud types

The gridded values for cloud occurrence frequencies (%) over the TP are displayed in Figure 3 for the monsoon season (May–Sep) and westerly season (Oct–Apr). Whereas most of the grid values exceed 70% for the monsoon months, the westerly season exhibits significantly lower values for all grid cells verifying that the plateau is much drier between October and April (Figure 3b) than between May and September (Figure 3a). Having said this, more than half of the sampled profiles are found to be cloudy during both seasons, indicating a generally high cloudiness over the whole region (Figure 3).

TABLE 2 Number of profiles in 2B-GEOPROF/2B-GEOPROF-LIDAR (2006–2011)

Domain	Day overpass	Night overpass	Total
Monsoon-dominated	254,354	252,347	506,701
Transition zone	825,414	824,772	1,650,186
Westerly dominated	595,436	598,725	1,194,161
Total	1,675,204	1,675,844	3,351,048

Table 3 shows the fractions of clouds detected in the datasets 2B-GEOPROF/2B-GEOPROF-LIDAR (2006–2011) for each subregion, divided into daytime versus nighttime and profiles with detected hydrometeors versus cloud profiles with detected cloud layers. The respective fractions of cloud layer occurrences in the data products 2C-ICE and 2B-CLDCLASS-LIDAR are now shown, since these encompass a 4-year (2007–2010) period which is already included in 2B-GEOPROF/2B-GEOPROF-LIDAR. The cloud detections differ hence at most 1% and show the same regional and diurnal variations as in 2B-GEOPROF/2B-GEOPROF-LIDAR. The table clarifies that the monsoon-dominated domain exhibits the highest percentages of detected clouds and cloud layers, followed by the westerly dominated domain. In general, cloud and cloud layer occurrence frequencies are higher during daytime than during nighttime, whereby the largest day–night differences occur in the transition zone.

Figure 4 shows the occurrence frequencies (%) for different types of detected cloud layers (in total 81% during the monsoon season and 64% during the westerly season) over the TP domain and the three subregions for the monsoon and westerly season based on 2B-CLDCLASS-LIDAR (2007–2010). The most frequent cloud types over the TP and in all three subregions are altostratus (As), stratocumulus (Sc) and cumulus (Cu) (cumulus congestus), whereby As refer to nonprecipitating cloud layers with base heights between 2 and 7 km above the surface and very little liquid water and Sc and Cu are clouds with base heights between 0 and 2 km above the surface (Wang and Sassen, 2007). Deep convective (DC) cloud layers occur only during the monsoon season and with frequencies below 3% in all three subregions. In general, stratiform cloud types (As and Sc) dominate the region but show also a clear seasonality and differences between the subregions. Whereas As is the most frequent cloud type in the transition zone (Figure 4e,f) and

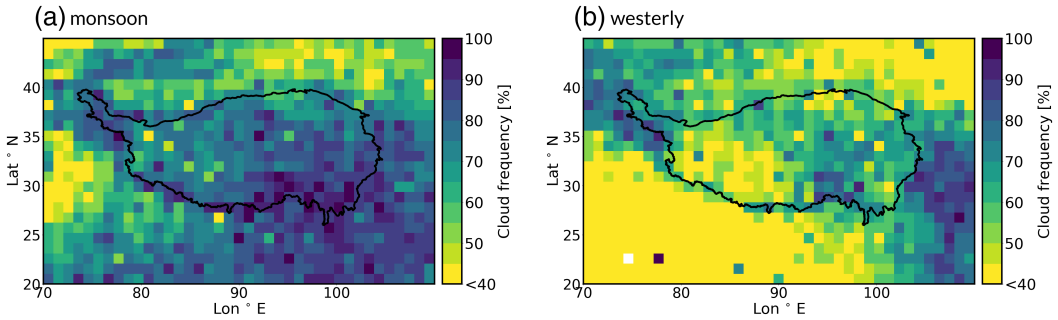

FIGURE 3 Cloud occurrence frequencies (%) over the TP for the (a) monsoon season (May–Sep) and (b) westerly season (Oct–Apr) based on 2B-GEOPROF and 2B-GEOPROF-LIDAR (2006–2011)

the westerly dominated domain (Figure 4g,h), Cu and Cr (Cirrus) are the most common cloud types in the monsoon-dominated domain (Figure 4c,d). The contribution of As in all subregions is generally higher during the westerly season (Figure 4b,d,f,g) and about 15% higher for the entire TP domain compared with the monsoon season. The monsoon season is, by contrast, characterized by an increased contribution of altocumulus and Cr (Figure 4a,c,e,g).

4.2 | Cloud vertical structure

The monthly variation of vertical cloud fractions based on 2B-GEOPROF/2B-GEOPROF-LIDAR (2006–2010), as shown in Figure 5, highlight once again the strong seasonality of cloud occurrences and indicate that the highest cloud fractions over the TP domain occur between 8 and 10 km a.s.l. from February to April and between 5 and 8 km a.s.l. during the monsoon season from May to September. This shows that the summer months are characterized by stronger cloud signals at lower levels above mean sea level, compared with the spring months where the troposphere above the TP is marked by hydrometeors at higher heights. The fact that the transition zone exhibits characteristics of both domains (Figure 5e,f) together with the spring peak of cloud fractions in the westerly dominated domain (Figure 5g,h) verify that the applied regional framework of Yao *et al.* (2013), implying precipitation peaks during spring in the northern TP, is reflected in the data. Day–night differences are most obvious in the monsoon-dominated domain, where high-level cloud fractions increase significantly during nighttime between June and August (Figure 5c,d). The two maxima of cloud fractions (5–8 km and 12–15 km a.s.l.) are disconnected, suggesting that the cloud peaks are associated with different cloud layer types rather than DC cells (Figure 5d). Recalling the retrieved cloud types for the monsoon-dominated domain during summer, this indicates the simultaneous occurrences of cirrus and lower convective clouds with small to moderate vertical extent.

It should be noted that the higher cloud fractions in the upper troposphere during nighttime do not depict that cloud layers or profiles containing hydrometeors are more frequent during night. Indeed, the opposite was found to be true (c.f. Section 4.1), so the higher cloud fractions during night reflect rather that CPR-detected hydrometeors and hence precipitation are more frequent (c.f. Section 3), but that the radar signals are detected from a smaller amount of cloudy profiles.

In addition to cloud fractions at different heights, we examined the normalized contoured-frequency-by-altitude diagram (CFAD) of radar reflectivities as derived from 2B-GEOPROF (2006–2011). The CFAD presents the number of occurrences in each height-reflectivity bin in relation to the total number of values in the cloudy profiles (Yuter and Houze Jr, 1995) and reveals thereby frequencies of particle

TABLE 3 Contribution of profile samples (%) from 2B-GEOPROF/2B-GEOPROF-LIDAR (2006–2011) which were found to be cloudy, separated into profiles which contain hydrometeors and profiles with at least one continuous cloud layer

Domain	Hydrometeors Daytime	Cloud layer Daytime	Hydrometeors Nighttime	Cloud layer Nighttime	Hydrometeors Total	Cloud layer Total
Monsoon-dominated	76	75	70	67	73	71
Transition zone	75	74	66	64	70	69
Westerly dominated	73	72	71	68	72	70
Total	75	74	68	66	72	70

Note: All cloud occurrences are displayed for different subregions and separated into day and nighttime.

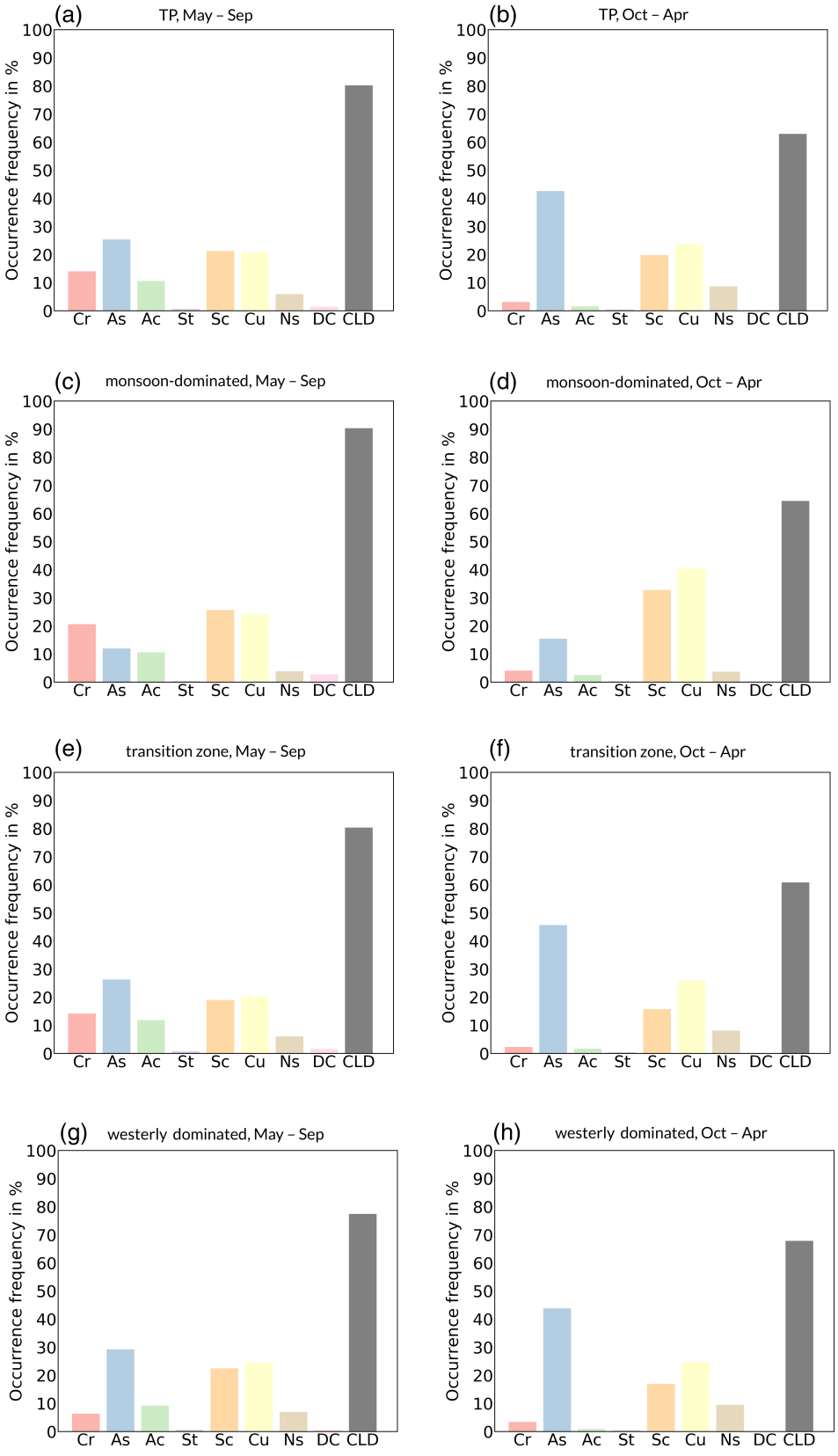

FIGURE 4 Relative occurrence frequencies (%) of different cloud types for TP domain (a–b), monsoon-dominated domain (c–d), transition zone (e–f) and westerly dominated domain (g–h) during the monsoon (May–Sep) and westerly season (Oct–Apr), based on 2B-CLDCLASS-LIDAR (2007–2010). The acronyms stand for following cloud types: Cr = cirrus, as = altostratus, ac = altocumulus, St = stratus, Sc = stratocumulus, cu = cumulus, ns = Nimbusstratus, DC = deep convection (layer base above 3 km above surface and large vertical extent), CLD = total cloud layer amount

sizes for different cloud altitudes (Figure 6). Both the seasonality of cloud characteristics as well as the regional dependence are well reflected in the radar reflectivity profiles: the two most distinct CFAD are the monsoon-dominated domain between May and September (Figure 6c) compared with the westerly dominated domain between

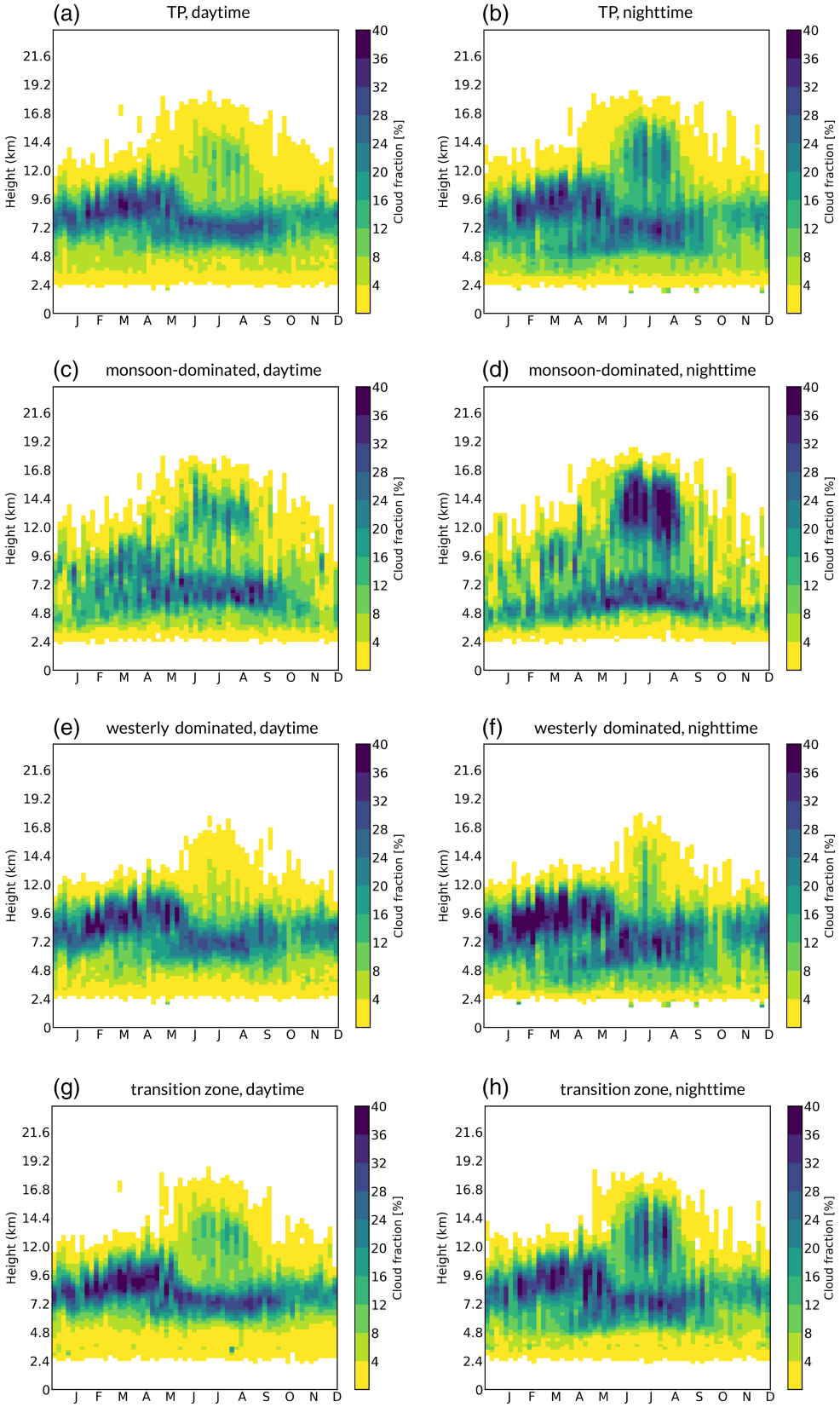

FIGURE 5 Monthly variation of vertical cloud fractions (%) for the TP domain (a–b), monsoon-dominated domain (c–d), westerly dominated domain (e–f) and transition zone (g–h) during daytime compared nighttime as derived from 2B-GEOPROF and 2B-GEOPROF-LIDAR (2006–2011). Cloud fractions include CPR and CALIOP detections and are presented as a 6-day average for each vertical profile bin (0.24 km)

October and April (Figure 6f). In general, differences between the westerly and monsoon season outweigh regional and day–night differences (not shown here), since both seasons entail two distinct radar reflectivity profiles which dominate the pattern in the TP domain as well as in each of the three subregions (Figure 6). The frequency values between −25 and −5 dBZ from 5 to 10 km a.s.l. increase significantly during the westerly season, resulting

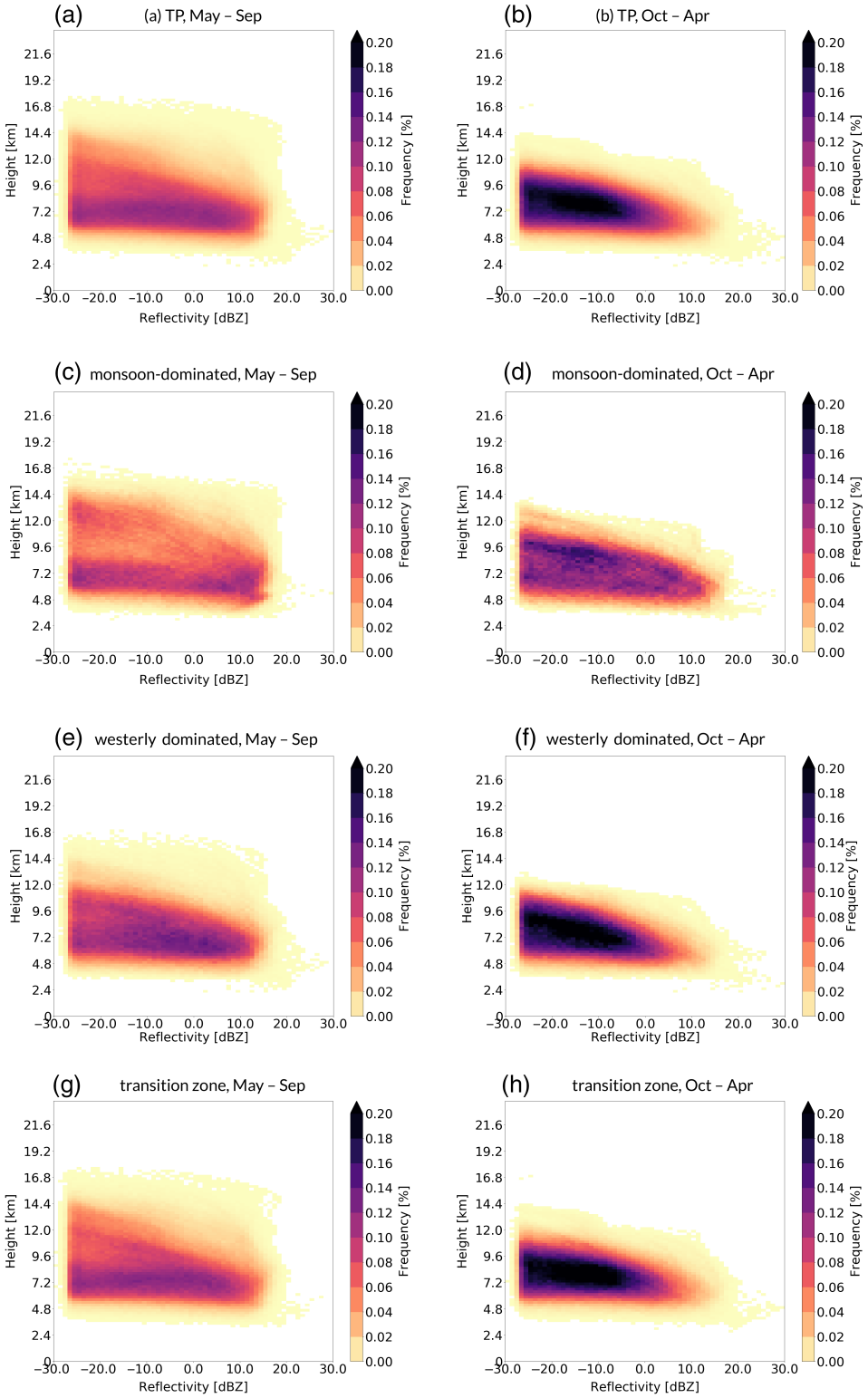

FIGURE 6 CFAD of radar reflectivity for TP domain (a–b), monsoon-dominated domain (c–d), westerly dominated domain (e–f) and transition zone (g–h) during monsoon (May–Sep) and westerly seasons (Oct–Apr) based on 2B-GEOPROF (2006–2011). The height bin (km a.s.l.) ranges from 2 to 17 km with a 0.24 km interval, and the reflectivity bin (dBZ) ranges from −30 to 30 dBZ with a 1 dBZ intervals

in a triangle-shaped CFAD (Figure 6b,d,f,h). The largest reflectivities during the westerly season occur below 7 km a.s.l., whereas lower reflectivity values which indicate smaller hydrometeors, are most frequent between 7 and 10 km a.s.l. All CFAD of the westerly season exhibit the highest frequencies for negative radar reflectivities and values above 10 dBZ are generally less frequent compared with the monsoon season. This reflects the drier westerly season (see also Figure 3), since precipitation is generally associated with higher radar reflectivity values. Meanwhile, frequency values in the monsoon season tend to be more spread over the height-reflectivity space, suggesting a higher variation of

particle sizes occurring at different levels (Figure 6a,c,e,g). This area-covering CFAD contrasts the bright-band dominated or triangle-shaped CFAD associated with the westerly circulation and implicates that cloud systems associated with the monsoon season tend to be more convective. In the westerly dominated domain during the westerly season, the dominant cloud systems are stratiform, which is consistent with the vertical cloud fractions and cloud types for the respective seasons and regions (Figures 4 and 5).

The higher variation of cloud layer types, cloud fractions and particle sizes at different heights during the monsoon (as shown in the previous section) is not necessarily attributed to single cloud layers during one satellite overpass, because CPR can detect up to five cloud layers in one sampled profile (Section 2). The frequencies of multiple cloud layers (% of all profiles which at least contain one cloud layer) are therefore presented in Figure 7. In general, single-layer clouds are the most frequent cloud layer type in the whole TP domain, contributing between 50 and 85% to the total cloud layer detections (Figure 7a). The relative contribution of single layer clouds shows a strong seasonal dependence in the monsoon-dominated south and decreases during the monsoon months, especially in July and August (Figure 7b). Multiple cloud layer occurrences are most frequent in the monsoon-dominated domain (Figure 7b) and during the monsoon months in all regions. The highest contribution of two-layer clouds are observed between May and September during night in the monsoon-dominated domain, which is consistent with the vertical cloud fractions revealing the co-occurrence of high-level cirrus clouds and low-level clouds in the summer nighttime profiles (c.f. Section 4.2). In the westerly dominated domain, two-layer clouds are most frequent in March (Figure 7d) and the transition zone shows again properties of both the westerly dominated and monsoon-dominated domain. The number of detected cloud layers during nighttime is smaller than that during daytime in all regions during all months (except for July in the monsoon-dominated domain). However, the nighttime curves for cloud layer amount frequencies follow the daytime curves and the monthly variation of cloud layer amount outweighs the day–night differences.

The PDF of cloud layer base height, top height and thickness (km), as shown in Figure 8, are examined for the monsoon-dominated domain during the monsoon season versus the westerly-domain during the westerly season, in order to obtain an indication of the vertical cloud structures that are associated with respective large-scale circulation. Both domains are dominated by low-level clouds with a small vertical extents, because more than 70% of the detected cloud layers reveal base heights between 0 and 3 km above the surface (Figure 8a,b) and thicknesses between 0 and 3 km (Figure 8e,f). This verifies the small

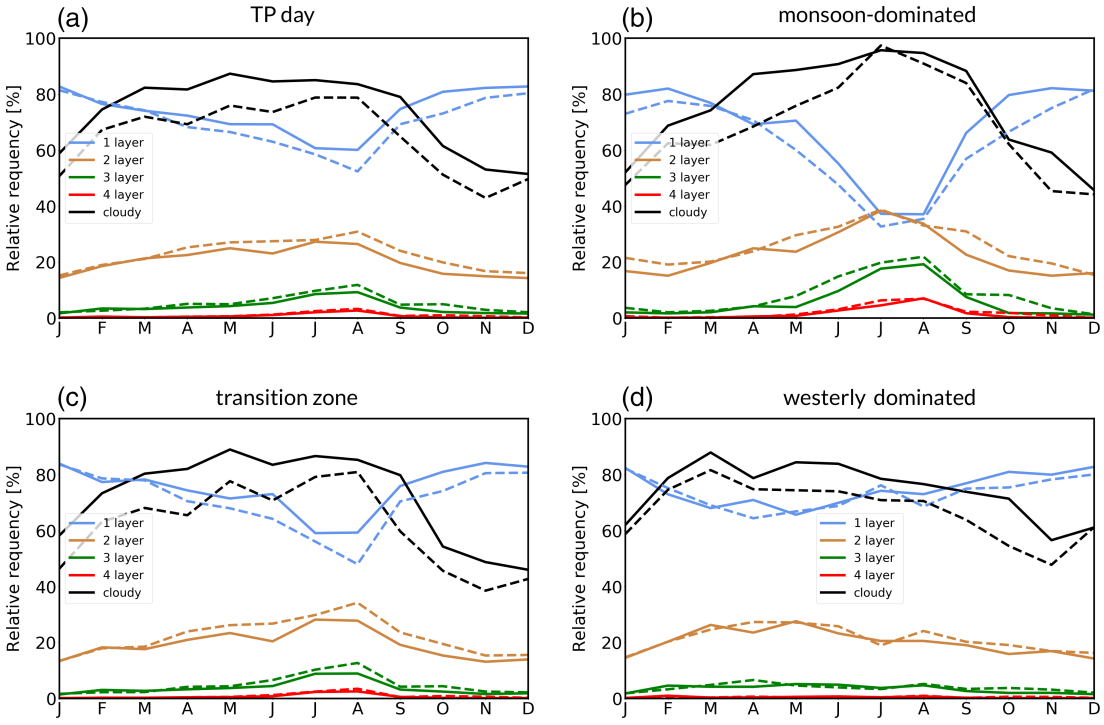

FIGURE 7 Monthly variation of detected cloud layer amount (% of profiles with at least one cloud layer) in the TP domain (a), monsoon-dominated domain (b), westerly dominated domain (c) and transition zone (d) based on 2B-CLDCLASS-LIDAR (2007–2010). The solid lines show the relative occurrence frequencies in daytime profiles and the dashed lines represent the nighttime profiles. The black curve refers to the occurrence frequency of samples that contain at least one detected cloud layer relative to all samples

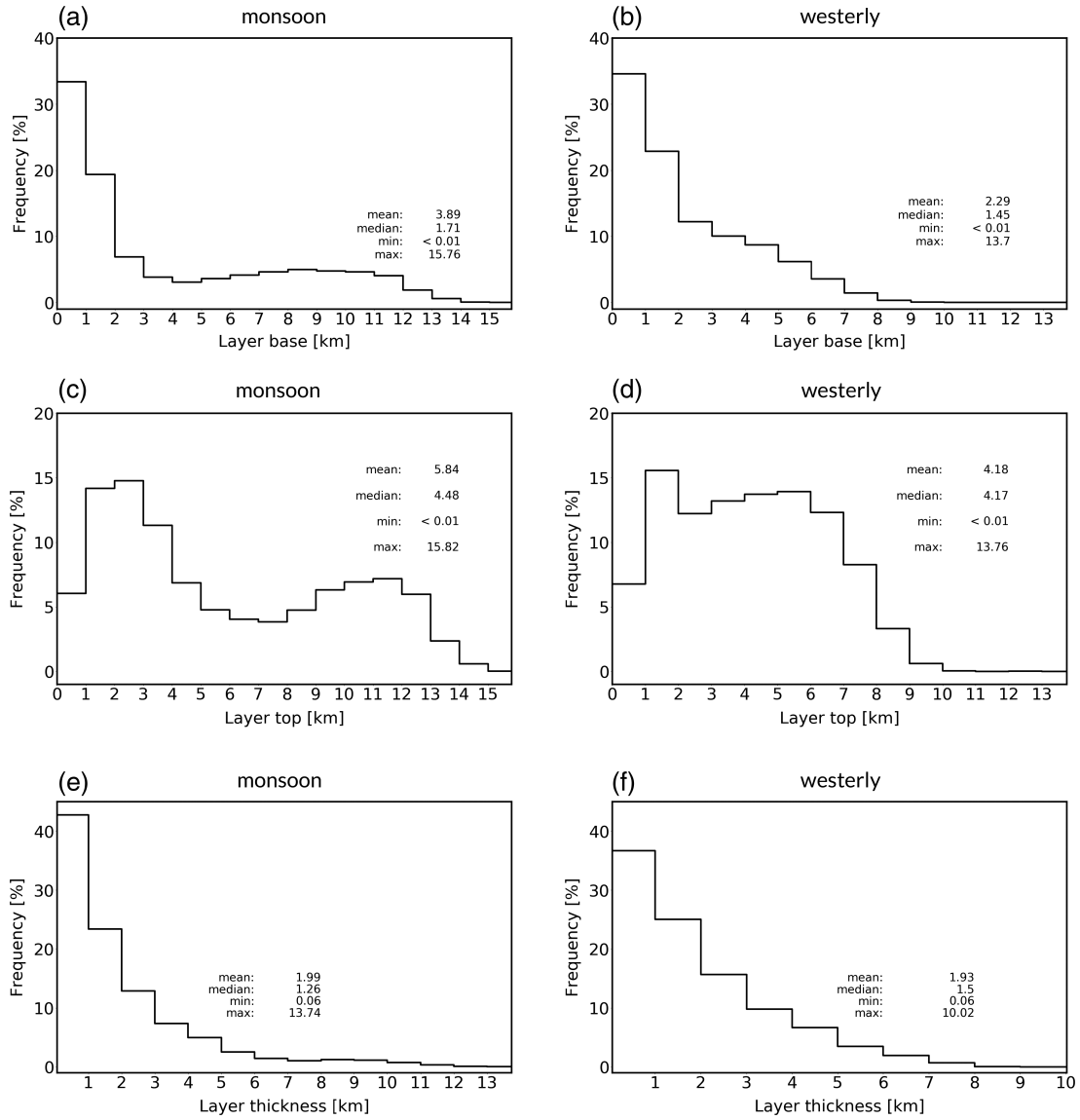

FIGURE 8 PDF of cloud layer base height, top height and thickness (km) for the monsoon-dominated domain during the monsoon season (a, c, e) and for the westerly dominated domain during the westerly season (b, d, f) based on 2B-CLDCLASS-LIDAR (2007–2010)

occurrence frequency of DC cloud layers (Figure 4) and suggests the high occurrence frequency of more stratiform cloud layers.

However, the monsoon-dominated domain during the monsoon season exhibits higher frequencies of larger base/-top heights and thicknesses as well as higher maxima compared with the layer properties associated with the westerlies. This means on one hand that convective cloud types are more frequent (as was displayed in Figure 4) and on the other hand that a significant fraction of clouds occur at higher heights, where ice clouds are more likely to occur. Interestingly, cloud top heights in the monsoon-dominated domain during the monsoon season reveal a bimodal distribution (Figure 8c) which also could be seen in the vertical cloud fraction profiles (Figure 5c). The two peaks of cloud top heights occur at 1–4 km and 9–12 km above the surface and can supposedly be attributed to cumulus clouds at lower levels and cirrus clouds at higher levels (Figure 4c).

4.3 | Ice clouds

As shown in the previous section, cloud layers over the TP show both seasonal and regional variations in vertical structure, which also has implications for its microphysical properties. Figure 9 shows the monthly variation of cloud particle phase by examining occurrence frequencies of ice, mixed-phase and liquid cloud layers over the TP and in the three subregions. Whereas more than 50% of cloud layers over the TP are ice clouds during the entire year, its contribution exceeds 80% between January and April (Figure 9a).

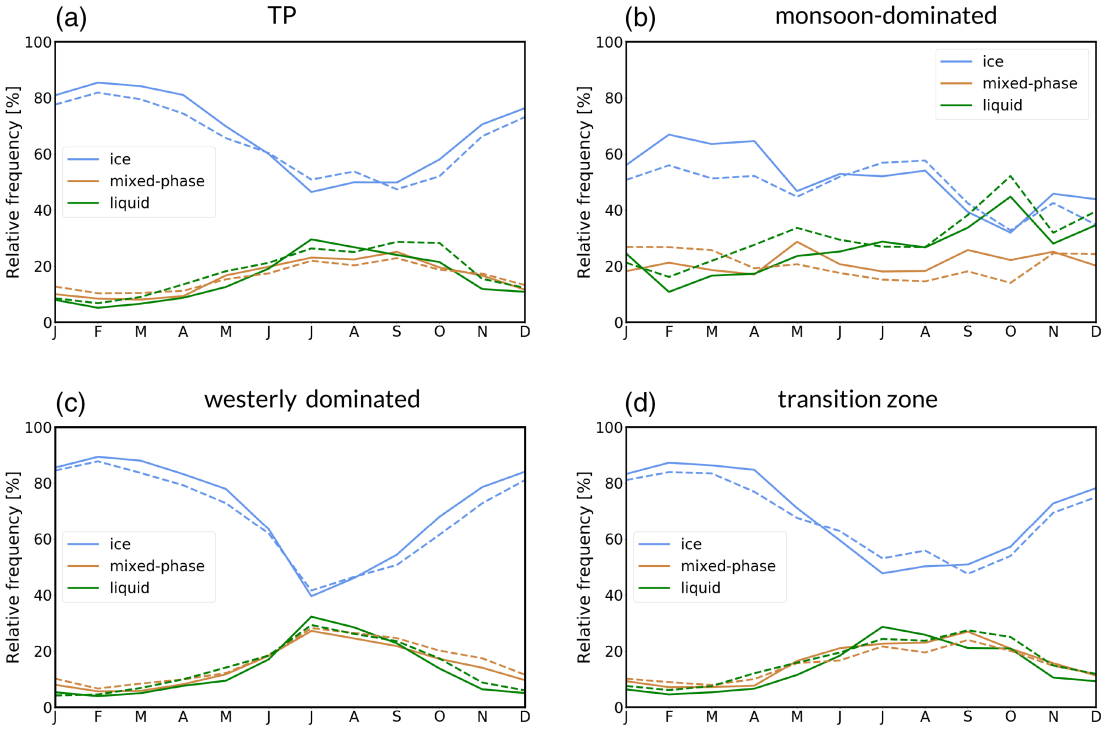

FIGURE 9 Monthly occurrence frequencies (%) of ice, liquid and mixed-phase cloud layers for the TP domain (a), monsoon-dominated domain (b), westerly dominated domain (c) and transition zone (d) based on 2B-CLDCLASS-LIDAR (2007–2010). The dashed line indicates the occurrence frequency of the respective cloud phase types during nighttime while the solid line describes the occurrence frequency of the cloud phase types during daytime

This shows clearly that ice cloud layers are the most frequent cloud phase type over the plateau, despite the seasonal and regional variations.

Liquid clouds peak between June and August in the westerly dominated domain and the transition zone (Figure 9c,d) and are most frequent in the monsoon-dominated domain, where more than 50% of the cloud layers are liquid clouds in October (Figure 9b). This result reflects also the higher occurrence of convective cloud types in the monsoon-dominated domain during the monsoon season (Figure 4c), since the liquid water content is generally higher for convective clouds. The monsoon season and the chosen monsoon-dominated domain of the TP point thus towards distinct signals in cloud characteristics with higher contributions of convective cloud types and lower contributions of ice clouds. Even though cloud occurrences are higher during the monsoon season and in the monsoon-dominated domain, the relative fractions of the most common cloud characteristics (including stratiform, ice and single-layer cloud layers) decrease, which means that hydrometeor sizes, cloud types and cloud macrophysical properties depict higher variations.

However, high-level cirrus clouds are, in contrast to the total amount of ice clouds, more frequent in the monsoon-dominated domain (Figure 4a,c,e), which means that ice clouds in the westerly dominated domain occur at lower levels. While cirrus clouds associated with the monsoon circulation are residues from deeper convective cells (Lau *et al.,* 2002), the ice clouds in the westerly region are classified as As clouds (Figure 4). This suggests different formation processes for cold cloud systems in the northern region of the TP, for example, lifting of more stable air masses in conjunction with warm frontal systems or descending cirrus cloud layers.

Moreover, the relative frequencies of ice, mixed-phase and liquid clouds in the subregions highlight the recurring characteristic of the transition zone showing more similar patterns to the westerly dominated domain than to the monsoon-dominated domain (Figure 9c,d).

Figure 10 displays average optical depth values during the monsoon versus the westerly season for all profiles (Figure 10a,b), profiles with cloud layer detections (Figure 10c,d) and profiles with liquid cloud layers (Figure 10e,f). While more than half of the optical depth values in the samples of the TP domain are between 0 and 1, its maximum values are above 300 for liquid cloud layers. Figure 10a–d show that the higher mean optical depth values during the monsoon season are also visible when only the optical depth values of the cloudy profiles are taken into account. This indicates that the reason for the higher optical depth values is not only the higher cloud occurrences in general but also due to the cloud properties. Figure 10e,f show evidence that the spatial pattern of mean optical depth values

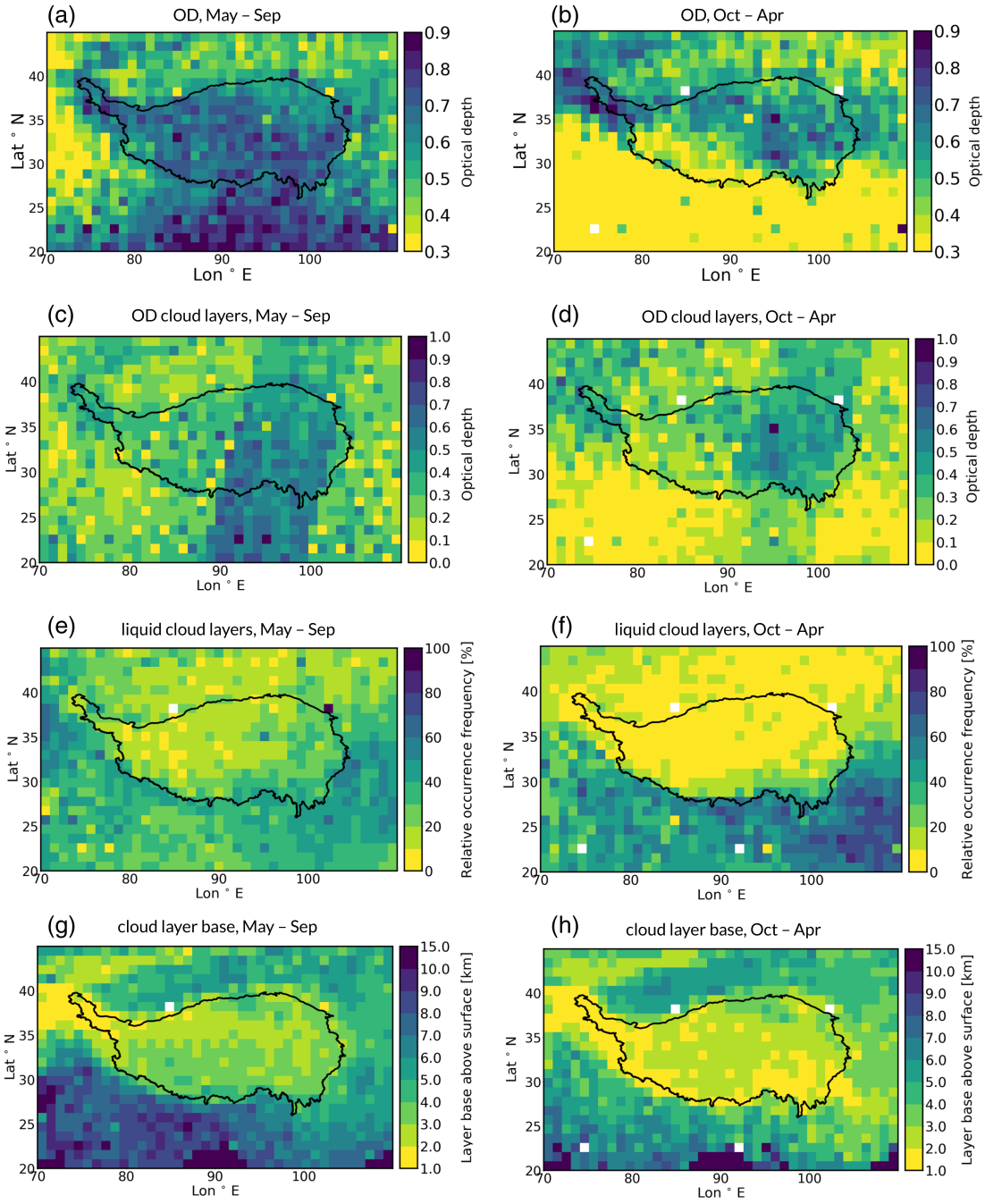

FIGURE 10 OD and cloud properties over the TP for the monsoon season (May–Sep) and (b) westerly season (Oct–Apr) based on 2C-ICE (2007–2010). Figure (a) and (b) display the seasonal mean optical depth, (c) and (d) the seasonal optical depth values when at least one cloud layer is present, (e) and (f) the seasonal relative occurrence frequency of liquid cloud layers and (g) and (h) the seasonal median cloud layer base height for detected cloud layers

is the same as for the contribution of liquid cloud layers. In addition, cloud layer bases above the surface are generally lower over the TP compared with the surrounding regions (Figure 10g,h). The higher occurrence frequency of ice and mixed-phase cloud layers at higher heights during the westerly season (c.f. Section 4.3) can therefore together with the generally lower cloud occurrence explain the lower mean optical depth. This effect is less pronounced at the southern edges of the TP and shows therefore once again both the seasonal and regional dependence of cloud properties over the TP.

The microphysical cloud properties associated with the monsoon circulation clearly reflect the linkage between large-scale circulation and cloud structure, because the monsoon circulation is associated with organized convection and the formation of meso-scale weather systems which in turn

result in higher occurrence frequencies of convective cloud cells (Lau *et al.,* 2002). These cloud systems triggered by organized vertical upward motion causes hence the higher contribution of liquid and mixed-phase cloud layers and larger optical thicknesses during the monsoon season.

5 | CONCLUSIONS AND DISCUSSION

In this study, seasonal and diurnal variations of cloud occurrences, cloud types, cloud vertical structure and ice clouds have been investigated and compared between three subregions of the TP. The results complement findings based on previous satellite observations and reveal significant differences in cloud characteristics between the examined seasons and regions. It was confirmed that low-level single-layer clouds generally dominate the TP during all seasons. Furthermore, three key features of spatial and temporal variations in clouds over the TP have been established: (a) the significant contribution of stratiform and ice clouds, (b) the distinct seasonality and (c) the well defined regional differences according to the framework of Yao *et al*. (2013). Since this study can serve as a pilot study to provide an overview of general variations in cloud properties, the elaborated key findings below can help to design future studies on convection processes and precipitation over the TP:

First, high occurrence frequencies of ice clouds and stratiform cloud types have been observed, especially in the westerly dominated north and during the westerly season. This implies that a strengthening of westerlies in the future could lead to an enhanced effect of ice clouds on the thermal forcing. Furthermore, the stratification of ice cloud layers can offer a possible mechanism for precipitation formation in addition to shallow convection, which could be important for the regional climate. We suggest therefore to further study the role of stratiform ice cloud layers for convection and precipitation.

Second, the monsoon season affects the TP in all three subregions and gives signals of increases in total cloud occurrences, liquid cloud layers and convective cloud types during the summer months. By taking advantage of the *CloudSat-CALIPSO* daytime and nighttime overpasses, diurnal variations have been compared with the seasonal variations. In general, the day–night differences are not as pronounced as variations between the westerly and monsoon season, even though hydrometeor and cloud layer occurrences during daytime are slightly higher than those during nighttime.

Third, significant differences in cloud characteristics between the monsoon-dominated and westerly dominated domains match with the differences associated with the respective seasons. During the monsoon season and in the monsoon-dominated south, higher variations in cloud types and cloud vertical structure could be observed due to the co-occurrence of high cirrus clouds and lower level cumulus. While both the monsoon season and the monsoon-dominated domain exhibit higher occurrence frequencies of low-level and convective cloud types with higher mean cloud thicknesses and optical depths, the dominating cloud type of the westerly dominated domain are ice clouds. This should be considered in future studies on changes in large-scale moisture transport and cloud feedbacks. Furthermore, the cloud characteristics in the westerly dominated domain appear to be closely linked with those in the transition zone, suggesting that the westerlies may have affected a larger region than assumed in the applied framework.

An important implication of these three key findings is that changes in large-scale circulation may result in altered cloud patterns. Increases in snowfall in the northern TP due to a strengthening of westerlies, as suggested by Deng *et al*. (2017), could for example lead to an even stronger domination of ice clouds, since the findings suggest that the westerly circulation associated with stratiform cold cloud types rather than convective cloud systems. When these ice clouds have high cloud top heights and low optical thicknesses, outgoing long-wave radiation is hampered, which enhances a positive cloud radiative effect and changes the heat budget through diabatic heating. Hence, future changes of westerlies and monsoon circulation may be crucial for cloud-radiation interactions, which at the current state are still dominated by a negative forcing and cooling effect (Yan *et al.,* 2016). In addition, changes in large-scale circulation will affect the geographical location of cyclogenesis and storm tracks, since these depend to a large extent on mean flow patterns (ref). The coupling between cloud micro- and macrophysical properties and large-scale features such as organized convection is, as confirmed by this study, associated with the monsoon circulation. This underlines the argument that changes in large-scale circulation patterns could significantly alter prevalent cloud regimes. However, the lower frequency of convective cloud structures in the drier northern TP does not mean that any organization of convection on a larger spatial scale is completely absent. Winter precipitation in the Himalayas, is partly attributed to Western Disturbances (Lang and Barros, 2004) and TP vortices (Wang, 1987), which are meso-scale weather systems originating in the region which in the applied framework belongs to the westerly dominated domain. How these systems can be linked to the observed cloud regimes in the northern TP, needs hence further consideration.

However, since this study also showed that clouds over the TP are highly heterogenous, different regions might be unequally sensitive to changes of hydro-climatic regimes. Kapnick *et al*. (2014) argue that precipitation over the

Karakoram region is, for example, much less sensitive to the observed warming than the Himalayas, because it is dominated by nonmonsoonal moisture transport. For monsoon-associated convection, it remains unclear which of the two following processes dominates: shallow convection which prevents the formation of large-scale stratiform precipitation (Li and Zhang, 2017) or the development of meso-scale convective systems during summertime (Yaodong *et al.,* 2008; Hu *et al.,* 2016, 2017) resulting in higher occurrence frequencies of deep convection cells and cirrus clouds. Since the magnitude of EDW in the TP region in the future will also depend on cloud properties (Pepin *et al.,* 2015), the relative importance of stratification, meso-scale convective systems and advection for cloud formation need to be quantified. An important milestone for this is, as could be shown by the distinct radar reflectivity profiles, the separation in convective and stratiform cloud systems according to a clear definition and based on vertical velocity (Houze Jr, 1997). In this way, the observed cloud systems which have been classified as stratiform here, could be allocated to different formation processes and more robust linkages between large-scale circulation and precipitation features could be established. In addition, microphysical processes, such as autoconversion, also feed back to the large-scale circulation through radiative–dynamic interactions by amplifying deep convection and convective-to-stratiform ratios in precipitation (Lau *et al.,* 2005). Since convective precipitation is generally more sensitive to warming (Berg *et al.,* 2013), increased frequencies of convective systems might enhance extreme precipitation events, particularly in the monsoon-dominated region.

The nocturnal precipitation peaks over the TP, which have been identified by several studies (Liang *et al.,* 2010; Bao *et al.,* 2011; Xu and Zipser, 2011; Xu *et al.,* 2012, Kukulies *et al*., unpublished manuscript), are not reflected in the day and nighttime cloud occurrence frequencies in the used data products, but as generally stronger CPR signals. This higher contribution of radar-detected compared with lidar-detected hydrometeors during night, indicates that nighttime precipitation is more intensive. An additional reason could be that the stronger radar reflectivities indicate larger fractions of snow and ice hydrometeors during night, for which CPR is fairly sensitive (Casella *et al.,* 2017) compared to drizzle and light rainfall during daytime, where more lidar-detected hydrometeors occur. This feature has been found to be most pronounced in the monsoon-dominated domain during summer, which could further reflect the maturity of meso-scale convective systems during late evening/night (Hu *et al.,* 2016), since most of these systems are associated with the southernmost regions of the TP (Hu *et al.,* 2017). In addition, the southeastern TP is, compared to the northwestern TP, characterized by higher frequency and intensity of hourly rainfall (Li, 2018), which is consistent with the general cloud features in the monsoon-dominated domain during summer: higher cloud frequencies and a higher contribution of convective clouds.

Using hourly summer precipitation data from 100 surface stations, Li (2018) identified two distinct modes of precipitation over the TP: late-afternoon peaks of shorter duration and midnight peaks of more intensive rainfall with longer duration. This "long-nighttime precipitation" leads to the expectation that more cloud layers during night should be detected by *CloudSat*, simply due to the higher probability of time matches between the satellite sampling and the precipitation occurrence. However, the fact that cloud layer occurrences and hydrometeor detections are lower during night could be due to the coarse temporal resolution of *CloudSat* and *CALIPSO*. (Fujinami *et al.,* 2005) determined a clear peak around 1800 LST (1000 UTC) for both cloud occurrence and precipitation frequencies based on both geostationary satellites and radar data and others point out midnight precipitation peaks over the TP (Liu *et al.,* 2009a; Bao *et al.,* 2011; Xu and Zipser, 2011). The *CloudSat* nighttime sample around 0230 LST (1830 UTC) might thus miss these precipitation peaks, whereas cloud layers associated with daytime surface heating and local thermal effects (Murakami, 1983) are captured more frequently. Another reasons for the discrepancy between maximum precipitation and highest frequencies of cloud layers could also be the strong dependence on local topography of hourly precipitation (Kurosaki and Kimura, 2002), which is not reflected in this study due to the focus on large-scale cloud features.

It should also be noted that the used datasets are global data products, so general retrieval assumptions might deviate from the climate conditions of the TP. In order to validate the importance of ice clouds in the TP region, the 2C-ICE product needs therefore to be calibrated with data from geostationary satellites. Furthermore, we suggest that the boundary of the westerly dominated zone of the TP can be more south, because the transition zone showed more similar cloud properties to the westerly dominated domain. The gridded data also revealed significant east–west differences in cloud properties, so the results of this paper together with Part 2 of the paper sequence and other comprehensive studies on cloud and precipitation regimes with a higher spatial resolution could be used to determine new borders for regions of large-scale impact (Yao *et al.,* 2013). Using only the cloud regimes for the determination of a new regional framework, is, however, not recommended, since precipitation features and moisture sources need to be considered. Moreover, the temporal resolution of *CloudSat* and *CALIPSO* is not be sufficient to identify a clear horizontal boundary of the regimes. This is reflected in the relatively small regional differences in the gridded visualization of

column-integrated values, whereby vertical and profile-based features exhibit clear regional differences.

Finally, the regional and seasonal division in this paper focuses on linkages between cloud formation and large-scale circulation. However, other factors such as aerosol forcing, local surface heating and local topography (Kurosaki and Kimura, 2002; Liu *et al.,* 2009a) can control convection features. As an example, Huang *et al*. (2007) found that a significant portion of dust aerosols from the Taklimakan Desert affects the TP during the summer months. Hence, the reason for the increase in cloud occurrences during summer in the westerly dominated domain and transition zone may not only indicate the transport of moisture and cloud systems by the monsoon circulation, but could also be attributed to higher surface temperatures resulting in more local convection and a higher availability of cloud condensation nuclei and ice condensation nuclei from dust aerosols.

ACKNOWLEDGEMENTS

This research was supported by the Strategic Priority Research Program of Chinese Academy of Sciences (Grant No. XDA20060401), Swedish National Space Agency (SNSA: 188/18) and Swedish STINT (Grant No. CH2015–6226), as well as Swedish National strategic research programs BECC and MERGE. M.W. is supported by the Ministry of Science and Technology of China (2017YFA0604002) and by the National Natural Science Foundation of China (No. 41575073, 41621005 and 91744208).

CONFLICT OF INTEREST

The authors declare no potential conflict of interest.

ORCID

Deliang Chen https://orcid.org/0000-0003-0288-5618

REFERENCES

Bao, X., Zhang, F. and Sun, J. (2011) Diurnal variations of warm-season precipitation east of the Tibetan Plateau over China. *Monthly Weather Review*, 139, 2790–2810.

Berg, P., Moseley, C. and Haerter, J.O. (2013) Strong increase in convective precipitation in response to higher temperatures. *Nature Geoscience*, 6, 181–185.

Berry, E. and Mace, G.G. (2015) Cloud properties and radiative effects of the Asian summer monsoon derived from A-Train data. *Journal of Geophysical Research: Atmospheres*, 119, 9492–9508.

Bibi, S., Wang, L., Li, X., Zhou, J., Chen, D. and Yao, T. (2018) Climatic and associated cryospheric, biospheric, and hydrological changes on the Tibetan Plateau: a review. *International Journal of Climatology*, 38, e1–e17.

Boucher, O., Randall, D., Artaxo, P., Bretherton, C., Feingold, G., Forster, P., Kerminen, V., Kondo, Y., Liao, H., Lohmann, U., Rasch, P., Satheesh, S., Sherwood, S., Stevens, B. and Zhang, X. (2013) Clouds and aerosols. In: Stocker, T.F., Qin, D., Plattner, G.-K., Tignor, M., Allen, S.K., Boschung, J., Nauels, A., Xia, Y., Bex, V. and Midgley, P.M. (Eds.) *Climate Change 2013: The Physical Science Basis. Contribution of Working Group I to the Fifth Assessment Report of the Intergovernmental Panel on Climate Change*. Cambridge, New York, NY: Cambridge University Press, pp. 866–871.

Casella, D., Panegrossi, G., Sanò, P., Marra, A.C., Dietrich, S., Johnson, B.T. and Kulie, M.S. (2017) Evaluation of the gpm-dpr snowfall detection capability: comparison with cloudsat-cpr. *Atmospheric Research*, 197, 64–75.

Chen, B. and Liu, X. (2005) Seasonal migration of cirrus clouds over the Asian monsoon regions and the Tibetan Plateau measured from MODIS/terra. *Geophysical Research Letters*, 32(1), L01804.

Deng, H., Pepin, N. and Chen, Y. (2017) Changes of snowfall under warming in the Tibetan plateau. *Journal of Geophysical Research: Atmospheres*, 122, 7323–7341.

Dong, W., Lin, Y., Wright, J.S., Ming, Y., Xie, Y., Wang, B., Luo, Y., Huang, W., Huang, J., Wang, L., Tian, L., Peng, Y. and Xu, F. (2016) Summer rainfall over the southwestern Tibetan Plateau controlled by deep convection over the indian subcontinent. *Nature Communications*, 7, 10925.

Duan, A. and Wu, G. (2006) Change of cloud amount and the climate warming on the Tibetan Plateau. *Geophysical Research Letters*, 33 (22), L22704.

Fujinami, H., Nomura, S. and Yasunari, T. (2005) Characteristics of diurnal variations in convection and precipitation over the southern Tibetan Plateau during summer. *Solaiat*, 1, 49–52.

He, Q., Li, C., Ma, J., Wang, H., Shi, G., Liang, Z., Luan, Q., Geng, F. and Zhou, X. (2013) The properties and formation of cirrus clouds over the tibetan plateau based on summertime lidar measurements. *Journal of the Atmospheric Sciences*, 70, 901–915.

Heymsfield, A.J., Winker, D. and van Zadelhoff, G.-J. (2005) Extinction-ice water content-effective radius algorithms for CALIPSO. *Geophysical Research Letters*, 32(10), L10807.

Houze, R.A., Jr. (1997) Stratiform precipitation in regions of convection: a meteorological paradox? *Bulletin of the American Meteorological Society*, 78, 2179–2196.

Hu, L., Deng, D., Gao, S. and Xu, X. (2016) The seasonal variation of Tibetan convective systems: satellite observation. *Journal of Geophysical Research: Atmospheres*, 121, 5512–5525.

Hu, L., Deng, D., Xu, X. and Zhao, P. (2017) The regional differences of Tibetan convective systems in boreal summer. *Journal of Geophysical Research: Atmosphere*, 122, 7289–7299.

Huang, J., Minnis, P., Yi, Y., Tang, Q., Wang, X., Hu, Y., Liu, Z., Ayers, K., Trepte, C. and Winker, D. (2007) Summer dust aerosols detected from CALIPSO over the Tibetan Plateau. *Geophysical Research Letters*, 34(18), L18805.

Kapnick, S.B., Delworth, T.L., Ashfaq, M., Malyshev, S. and Milly, P. C. (2014) Snowfall less sensitive to warming in karakoram than in himalayas due to a unique seasonal cycle. *Nature Geoscience*, 7, 834–840.

Kurosaki, Y. and Kimura, F. (2002) Relationship between topography and daytime cloud activity around Tibetan Plateau. *Journal of the Meteorological Society of Japan. Ser. II*, 80, 1339–1355.

Lang, T.J. and Barros, A.P. (2004) Winter storms in the central himalayas. *Journal of the Meteorological Society of Japan. Ser. II*, 82, 829–844.

Lau, K., Wu, H., Sud, Y. and Walker, G. (2005) Effects of cloud microphysics on tropical atmospheric hydrologic processes and intraseasonal variability. *Journal of Climate*, 18, 4731–4751.

Lau, K.-M., Li, X. and Wu, H. (2002) Evolution of the large scale circulation, cloud structure andregional water cycle associated with the South China Sea monsoonduring May-June, 1998. *Journal of the Meteorological Society of Japan. Ser. II*, 80, 1129–1147.

Li, J. (2018) Hourly station-based precipitation characteristics over the tibetan plateau. *International Journal of Climatology*, 38, 1560–1570.

Li, Y. and Zhang, M. (2016) Cumulus over the Tibetan Plateau in the summer based on Cloudsat–CALIPSO data. *Climate*, 29, 1219–1230.

Li, Y. and Zhang, M. (2017) The role of shallow convection over the Tibetan Plateau. *Journal of Climate*, 30, 5791–5803.

Liang, H., Yang, S., Li, Y.D. and Gao, S.T. (2010) Diurnal variability of precipitation depth over the Tibetan Plateau and its surrounding regions. *Advances in Atmospheric Sciences*, 27, 115–122.

Liu, W., Wang, L., Chen, D., Tu, K., Ruan, C. and Hu, Z. (2016) Large-scale circulation classification and its links to observed precipitation in the eastern and central Tibetan Plateau. *Climate Dynamics*, 46, 3481–3497.

Liu, X., Bai, A. and Liu, C. (2009a) Diurnal variations of summertime precipitation over the Tibetan Plateau in relation to orographically-induced regional circulations. *Environmental Research Letters*, 4, 045203.

Liu, X., Cheng, Z., Yan, L. and Yin, Z.-Y. (2009b) Elevation dependency of recent and future minimum surface air temperature trends in the tibetan plateau and its surroundings. *Global and Planetary Change*, 68, 164–174.

Luo, Y., Zhang, R., Qian, W., Luo, Z. and Hu, X. (2011) Intercomparison of deep convection over the Tibetan Plateau–Asian Monsoon Region and subtropical North America in boreal summer using CloudSat/CALIPSO data. *Journal of Climate*, 24, 2164–2177.

Mace, G. (2008) *A Nasa Earth System Science Pathfinder Mission, Cloudsat Standard Data Products Handbook. Cooperative Institute for Research in the Atmosphere*. Fort Collins, CO: Colorado State University.

Mace, M. and Deng, M. (2011) Level 2 CloudSat-CALIPSO Combined Ice Cloud Property Retrieval Product Process Description Document. *NASA CloudSat Project Rep.*

Murakami, M. (1983) Analysis of the deep convective activity over the western pacific and southeast asia. *Journal of the Meteorological Society of Japan. Ser. II*, 61, 60–76.

Pan, Z., Mao, F., Gong, W., Min, Q. and Wang, W. (2017) The warming of Tibetan Plateau enhanced by 3d variation of low-level clouds during daytime. *Remote Sensing of Environment*, 198, 363–368.

Pepin, N., Bradley, R., Diaz, H., Baraër, M., Caceres, E., Forsythe, N., Fowler, H., Greenwood, G., Hashmi, M., Liu, X., Miller, J.R., Ning, L., Ohmura, A., Palazzi, E., Rangwala, I., Schöner, W., Severskiy, I., Shahgedanova, M., Wang, M.B., Williamson, S.N. and Yang, D.Q. (2015) Elevation-dependent warming in mountain regions of the world. *Nature Climate Change*, 5, 424.

Ruethrich, F., Thies, B., Reudenbach, C. and Bendix, J. (2013) Cloud detection and analysis on the Tibetan Plateau using Meteosat and CloudSat. *Journal of Geophysical Research-Atmospheres*, 118, 10082–10099.

Sassen, K. and Wang, Z. (2008) Classifying clouds around the globe with the cloudsat radar: 1-year of results. *Geophysical Research Letters*, 35(4), L04805.

Shang, H., Letu, H., Nakajima, T.Y., Wang, Z., Ma, R., Wang, T., Lei, Y., Ji, D., Li, S. and Shi, J. (2018) Diurnal cycle and seasonal variation of cloud cover over the tibetan plateau as determined from himawari-8 new-generation geostationary satellite data. *Scientific Reports*, 8, 1105.

Stephens, G.L., Vane, D.G., Boain, R.J., Mace, G.G., Sassen, K., Wang, Z., Illingworth, A.J., O'Connor, E.J., Rossow, W.B., Durden, S.L., Miller, S.D., Austin, R.T., Benedetti, A., Mitrescu, C. and CloudSat Science Team. (2002) The CloudSat mission and the a-train: A new dimension of space-based observations of clouds and precipitation. *Bulletin of the American Meteorological Society*, 83, 1771–1790.

Wang, B. (1987) The development mechanism for tibetan plateau warm vortices. *Journal of the Atmospheric Sciences*, 44, 2978–2994.

Wang, B. (2002) Rainy season of the asian–pacific summer monsoon. *Journal of Climate*, 15, 386–398.

Wang, Z. and Sassen, K. (2007) Level 2 cloud scenario classification product process description and interface control document. *Version*, 5, 50.

Winker, D.M., Vaughan, M.A., Omar, A., Hu, Y., Powell, K.A., Liu, Z., Hunt, W.H. and Young, S.A. (2009) Overview of the calipso mission and caliop data processing algorithms. *Journal of Atmospheric and Oceanic Technology*, 26, 2310–2323.

Xu, J., Zhang, B., Wang, M. and Wang, H. (2012) Diurnal variation of summer precipitation over the Tibetan Plateau: a cloud-resolving simulation. *Annales Geophysicae*, 30, 1575–1586.

Xu, W. and Zipser, E.J. (2011) Diurnal variations of precipitation, deep convection, and lightning over and east of the eastern Tibetan Plateau. *Journal of Climate*, 24, 448–465.

Yan, Y., Liu, Y. and Lu, J. (2016) Cloud vertical structure, precipitation, and cloud radiative effects over Tibetan Plateau and its neighboring regions. *Journal of Geophysical Research: Atmospheres*, 121, 5864–5877.

Yan, Y.-F., Wang, X.-C. and Liu, Y.-M. (2017) Cloud vertical structures associated with precipitation magnitudes over the Tibetan Plateau and its neighboring regions. *Atmospheric and Oceanic Science Letters*, 11(1), 44–53.

Yao, T., Masson-Delmotte, V., Gao, J., Yu, W., Yang, X., Risi, C., Sturm, C., Werner, M., Zhao, H., He, Y., Ren, W., Tian, L., Shi, C. and Hou, S. (2013) A review of climatic controls on δ18o in precipitation over the Tibetan Plateau: observations and simulations. *Reviews of Geophysics*, 51, 525–548.

Yao, T., Thompson, L.G., Mosbrugger, V., Zhang, F., Ma, Y., Luo, T., Xu, B., Yang, X., Joswiak, D.R., Wang, W., Joswiak, M.E., Devkota, L.P., Tayal, S., Jilani, R. and Fayziev, R. (2012) Third pole environment (tpe). *Environmental Development*, 3, 52–64.

Yao, T., Xue, Y., Chen, D., Chen, F., Thompson, L., Cui, P., Koike, T., Lau, W.K.-M., Lettenmaier, D., Mosbrugger, V., Zhang, R., Xu, B., Dozier, J., Gillespie, T., Gu, Y., Kang, S., Piao, S., Sugimoto, S., Ueno, K., Wang, L., Wang, W., Zhang, F., Sheng, Y., Guo, W., Ailikun, X.Y., Ma, Y., Shen, S.S.P., Su, Z., Chen, F., Liang, S., Liu, Y., Singh, V.P., Yang, K., Yang, D.,

Zhao, X., Qian, Y., Zhang, Y. and Li, Q. (2018) Recent third pole's rapid warming accompanies cryospheric melt and water cycle intensification and interactions between monsoon and environment: multi-disciplinary approach with observation, modeling and analysis. *Bulletin of the American Meteorological Society*, 100(3), 423–444.

Yaodong, L., Yun, W., Yang, S., Liang, H. and Shouting, G. (2008) Characteristics of summer convective systems initiated over the Tibetan plateau. Part i: origin, track, development, and precipitation. *Journal of Applied Meteorology and Climatology*, 47, 2679–2695.

Yuter, S.E. and Houze, R.A., Jr. (1995) Three-dimensional kinematic and microphysical evolution of Florida cumulonimbus. Part i: spatial distribution of updrafts, downdrafts, and precipitation. *Monthly Weather Review*, 123, 1921–1940.

Zhang, Y., Chen, H. and Yu, R. (2014) Vertical structures and physical properties of the cold-season stratus clouds downstream of the Tibetan Plateau: differences between daytime and nighttime. *Journal of Climate*, 27, 6857–6876.

How to cite this article: Kukulies J, Chen D, Wang M. Temporal and spatial variations of convection and precipitation over the Tibetan Plateau based on recent satellite observations. Part I: Cloud climatology derived from *CloudSat* and *CALIPSO*. *Int J Climatol*. 2019;1–17. https://doi.org/10.1002/joc.6162